CHAPTER 6 ENERGY AREA

TiO_2-WO_3 HETEROJUNCTIONS FOR PHOTOCATALYTIC HYDROGEN GENERATION

X. González-Bautista[1], M. L. Hernández-Pichardo[2*], J. V. Méndez -Méndez[3*]

[1]Instituto Politécnico Nacional, Escuela Nacional de Ciencias Biológicas (ENCB), UPALM, C.P. 07738, CDMX, México.

[2]Instituto Politécnico Nacional, Laboratorio de nanomateriales sustentables, Escuela de Ingeniería Química e Industrias Extractivas (ESIQIE), UPALM, C.P. 07738, CDMX. México.

[3]Instituto Politécnico Nacional – Centro de Nanociencias y Micro y Nanotecnologías Luis Enrique Erro s/n, C. P, 07738, CDMX. México.

* mhernandezp@ipn.mx, jmendezm@ipn.mx

Abstract

Clean energy and water pollution are significant challenges that demand innovative solutions. Photocatalysis, as an emerging technology, holds the potential to address these issues. In our research, we have synthesized TiO_2 nanosheets and a composite based on a TiO_2-WO_3 heterojunction using a hydrothermal method. Different characterization techniques were used, and the formation of the anatase phase directly interacting with WO_x clusters was observed. In samples prepared with WO_3, the presence of the W=O vibrational mode was observed, and TEM studies confirmed the formation of the heterojunction between TiO_2 and WO_3. The higher H_2 production is attributed to the formation of this heterojunction, which inhibits the recombination of electrons and holes. The bandgap of the TiO_2-WO_3 catalysts was slightly smaller than that of pristine TiO_2. The heterojunction formation inhibits the e^-/h^+ recombination rate, thus favoring the separation of photoproduced carriers. The TW5 catalyst demonstrated the highest production rate, reaching 663.54 $\mu mol \cdot g^{-1}$ within 4 hours. These findings underscore the potential of TiO_2-WO_3 heterojunctions in the field of photocatalytic hydrogen production, inspiring further research and development in this area.

Keywords: TiO_2-WO_3 heterojunction, photocatalysis, hydrogen production

1. Introduction

The US Academy of Sciences report [1] indicates that global energy consumption is projected to increase by two and three times in 2050 and 2100 compared to 2001 (13.5 TW). This forecast reflects a challenging scenario that calls for urgent action to avoid a major energy crisis with the least possible environmental impact. Against this background, it has become imperative to explore and develop alternative energy sources that are clean, renewable, economically viable, and sustainable as an alternative to traditional fossil fuels to meet the growing energy demands of human society. In this context, hydrogen stands out as a regenerative and environmentally friendly energy carrier, attracting significant attention from the scientific community in recent decades. However, the current hydrogen production process, which mainly derives from fossil fuels through natural gas steam reforming processes, raises significant concerns regarding sustainability and the negative environmental impact. These challenges underscore the importance of our research in proposing a solution to these issues. Therefore, future hydrogen generation is anticipated to be based on harnessing renewable energy sources [2].

Solar energy is a promising option for effectively addressing global energy challenges in this context. Photocatalytic hydrogen production through solar and semiconductor-driven water splitting has emerged as a key strategy to address both solar energy storage and green hydrogen production [3 - 5]. However, this approach presents significant challenges, particularly in identifying highly efficient and stable visible-light active photocatalysts capable of providing excited charge carriers for H_2 or O_2 evolution reactions under visible light irradiation.

In this regard, tungsten trioxide (WO_3) has emerged as a promising co-catalyst due to its light absorption properties at wavelengths up to 480 nm, its relatively narrow bandgap (approximately 2.8 eV), and its stability and safety under acidic and oxidative conditions [5, 6]. Furthermore, tungsten oxide (WO_3) exhibits a high gap mobility of 10 $cm^2\ V^{-1}\ s^{-1}$ and a gap migration distance of 150 nm. This facilitates charge separation in the TiO_2-WO_3 heterojunction. The combination of these materials forms a perfect interface, thanks to the similarity in ionic radius (Ti^{4+}: 0.0605 nm; W^{6+}: 0.0600 nm) and metal-to-metal distance (Ti-Ti: 3.78 Å; W-W: 3.84 Å) [7].

This study is focused on optimizing the interaction between titanium oxide and tungsten oxide by forming nanosheets and/or nanobelts to increase the

charge transport efficiency. The optimization is based on the morphology, which allows a linear passage of the charge carriers along two-dimensional planes. This improves the photocatalytic activity by extending the absorption range of TiO_2 through heterojunction with WO_3.

2. Experimental Methodology

2.1. *Synthesis of Titanium Dioxide (TiO_2) by the hydrothermal method*

The synthesis of TiO_2 was carried out using a process described in [8]. Briefly, 12.5 mL of $C_{16}H_{36}O_4Ti$ (titanium (IV) butoxide) and 1.5 mL of hydrofluoric acid (70 wt.%) were added, and the mixture was stirred for 2 h until a gel was obtained. The gel was transferred to a Teflon autoclave and kept at 180 °C for 36 h. After cooling, the product was washed with ethanol and distilled water several times. Subsequently, the product was dispersed in a 0.01 M NaOH solution and stirred for 8h. The precipitate was recovered by centrifugation at high speed, washed with distilled water and ethanol several times, and dried at 80 °C for 6 h.

2.2. *Synthesis of TiO_2-WO_3 catalysts (TW) by the hydrothermal method*

The synthesis of TiO_2-WO_3 was performed using a hydrothermal method. The following materials were used: 12.5 mL of $C_{16}H_{36}O_4Ti$, AMT (ammonium metatungstate) at 5, 10, and 15 wt.% with respect to WO_3, and 1 mL of hydrofluoric acid (70 wt.%). These were added and kept under stirring for 2 h. The gel was transferred to a Teflon autoclave and kept at 180 °C for 36 h. After cooling, the product was cooled. Once cooled, the product was washed with ethanol and distilled water several times. Subsequently, the product was dispersed in a 0.01 M NaOH solution and stirred for 8 h. The precipitate was recovered by centrifugation. The precipitate was recovered by centrifugation, washed with distilled water and ethanol several times, and dried at 80 °C for 6 h.

2.3. *Photocatalytic activity tests*

The photocatalytic behavior of the samples for the generation of H_2 was carried out using a water/methanol solution under UV irradiation. In a typical experiment, 0.1 g of photocatalyst is dispersed in 150 mL of water/methanol solution (1:1 volume). A Pen Ray Hg UV lamp (254 nm, 4.4 mW/cm^2) is used to irradiate the

solution. The products were identified using a Perkin-Elmer model Clarus 480 chromatograph. H_2 evolution was monitored by online gas chromatography.

The photocatalytic degradation of methyl orange (MO) was carried out in a photoreactor (Photo Q 200 brand Prendo), using a concentration of 20 mg/L of MO and 100 mg of catalyst. Before illumination, the suspension was magnetically stirred in the dark for 30 min to establish adsorption-desorption equilibrium at room temperature. Subsequently, the sample is subjected to UV-Vis light irradiation (UV-C ~400 nm). Sampling was carried out at regular time intervals.

3. Results and discussion

3.1. *Structural and textural properties of photocatalysts*

Figure 1 shows the diffractogram of the catalysts. The T0 sample exhibited peaks at 2θ = 25.33, 36.99, 37.83, 38.63, 48.07, 53.93, 55.09, 62.13, 62.73, 68.79, 70.31, 75.07 and 76.09 degrees (JCPDS No. 21-1272) [9, 10], and it is possible to observe traces of the rutile phase (2θ = 27.45º). Additionally, the sample has been found to exhibit high crystallinity, with a crystal size of 32 nm obtained from Scherrer's equation (1).

$$D = \frac{K \cdot \lambda}{\beta \cos\theta} \quad (1)$$

For TW5, TW10 and TW15 catalysts, it was observed that the anatase phase of titania predominates, as indicated by peaks around 2θ = ~25.30, 38.01, 48.01, 53.93, 54.97, 62.71, 68.83, 70.19, 75.11 y 75.93 degrees (JCPDS No. 89-4921) [11]. The absence of WO_3 signals indicates that tungsten nanostructures may exist in sizes smaller than 3 nm. Furthermore, the TW catalysts exhibit comparable crystallinity, although it is less pronounced than that of T0. Concurrently, it was observed that the crystallite size of the samples with tungsten oxide decreased as the tungsten oxide content increased. The crystallite sizes were 13, 10, and 8 nm for samples TW5, TW10, and TW15, respectively.

It is important to note that the catalysts were not subjected to additional heat treatment. This is because such a process involves a higher energy consumption during preparation. It is important to note that hydrothermal synthesis allows for direct control of reaction conditions. Consequently, there is no need to use calcination or other similar treatment methods to obtain crystallized products, as this synthesis method provides crystalline and uniform products [12].

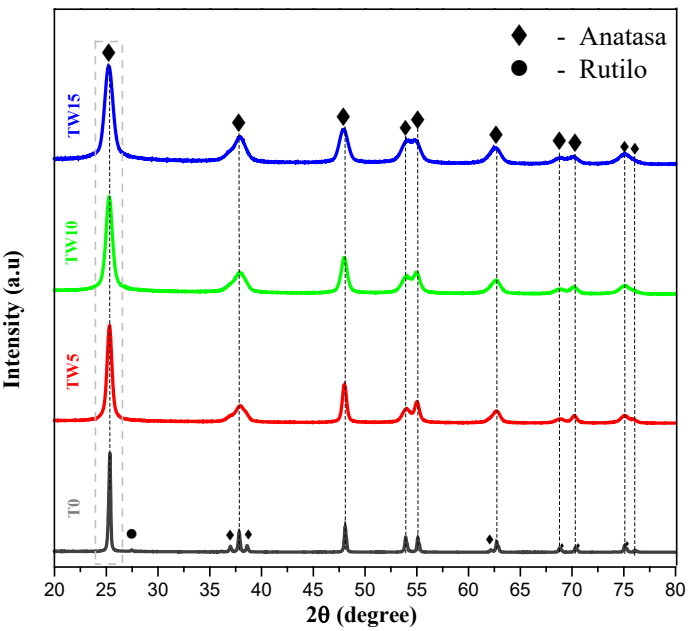

Figure 1. Diffractogram of the TiO_2 and TiO_2-WO_3 samples.

Figure 2 shows the Raman spectra of the T0 samples in comparison to the TW catalysts. In the case of the T0 sample, we can observe the characteristic vibrational modes of titania, which are 142, 196, 396, 517, and 639 cm^{-1}. The 142, 517, and 639 cm^{-1} modes correspond to the O-Ti-O bond vibrations, the 196 cm^{-1} mode to O-Ti, and the 396 cm^{-1} mode to Ti-O [13, 14]. For samples TW5, TW10, and TW15, we observed the characteristic vibrational modes of titania.

In the case of sample TW5, we did not observe the presence of WO_x nanostructures, but we did observe a characteristic signal at 966 cm^{-1} only for samples TW10 and TW15. The signal corresponds to the stretching mode of the terminal W=O double bonds present in WO_x clusters (Figure 2b) [15]. The 966 cm^{-1} signal of the TW10 and TW15 catalysts becomes broader and weaker as the WO_3 content increases. This could indicate an increase in defects in the titania crystal lattice [16], favoring the capture of photogenerated electrons and inhibiting the recombination of e^-/h^+ [15]. At the same time, we observed a shift towards higher frequencies of the main TiO_2 signal at 142 cm^{-1}, especially in the TW catalysts. This shift could indicate the formation of a heterojunction between TiO_2 and WO_3, which would result in certain changes in the titania structure due to the incorporation and increase in %wt. of WO_3 [11].

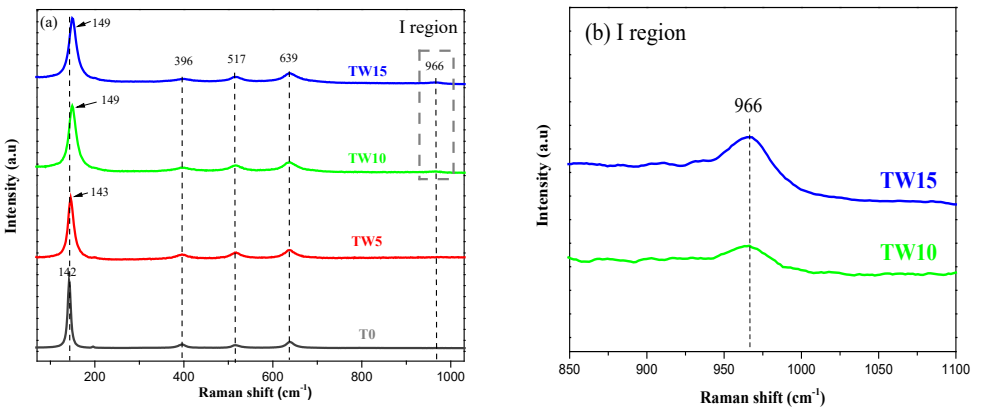

Figure 2. a) Raman spectra of catalysts T0 and TW; b) Magnified view of region I.

The morphologies of the T0 and TW catalyst samples were observed by SEM. Figure 3 shows the morphology of T0; we can observe a morphology of agglomerates with irregular structures; its EDS revealed the presence of Ti, O, and impurity of Si, which is attributable to the synthesis method of the distributor.

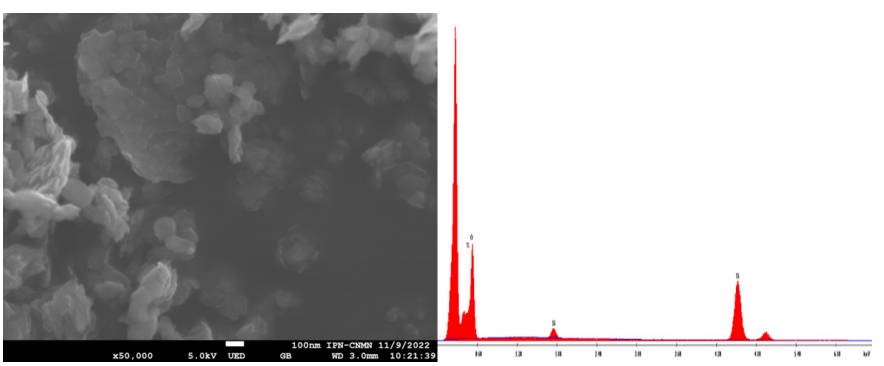

Figure 3. SEM images of sample T0 and EDS results.

In Figure 4, we can observe the morphology of the TW catalysts; in the case of TW5 (Figure 4A), aggregates and agglomerates are observed, but no defined morphology was observed for this catalyst. In Figure 4B, we can observe the morphology of the TW10 catalyst; again, we observe agglomerates without any type of morphology in the same way it is observed for the TW15 catalyst (Figure 4C). We can suggest that this type of irregularly shaped aggregate is due to the failure to develop crystals [17], and this can be observed with XRD (Figure 1), as the crystalline phases of WO_3 were not observed, suggesting that WOx may be grown from small TiO_2 structures. The EDS results for the TW catalysts identified and confirmed the presence of O, F, Ti, and W. The uniform

distribution of the O, Ti, and W elements of each TW catalyst detected by EDS can also be seen below.

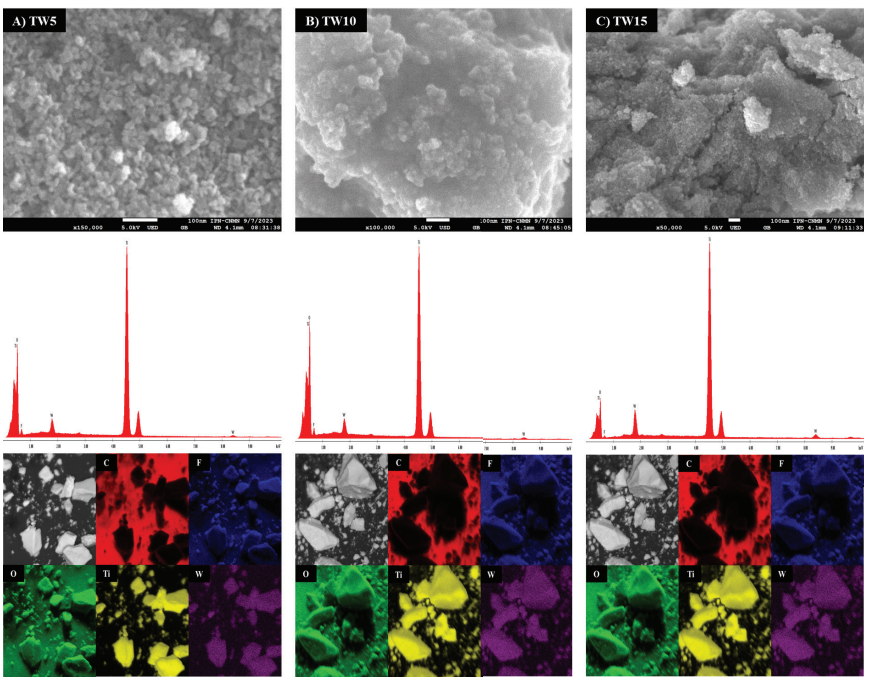

Figure 4. SEM images of A) TW5, B) TW10, and C) TW15, and EDS and mapping results (bottom).

Figure 5 shows the TEM images of the TiO_2-WO_3 samples, it shows the effect of the tungsten oxide on the particle size (Figures 5a-5c). It is observed that the particle size is decreasing as the tungsten oxide is increasing. Also, Fig 5d. shows the HAADF images of the TW5 sample showing the typical formation of the TiO_2-WO_3 heterojunction. The WO_3 phase is present as small WOx clusters, as is observed in the HAADF images as brighter spots corresponding to tungsten atoms deposited on the TiO_2 crystals ensuring intimate contact between the two phases.

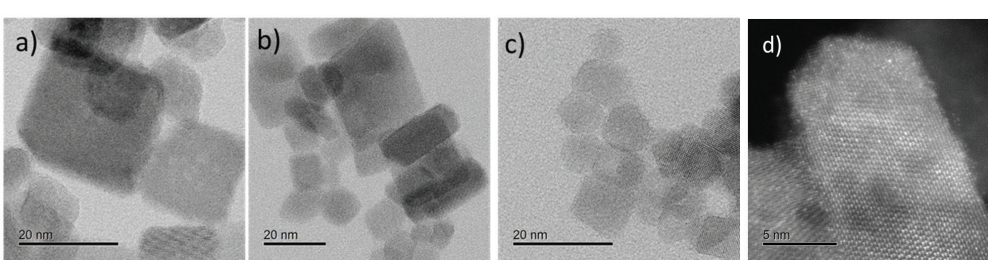

Figure 5. HRTEM images of the TW5. TW10 and TW15 samples (5a, 5b, and 5c, respectively) and HAADF images of the TW5 sample.

3.2. *Band gap*

The Tauc model was used to determine the optical band gap energy of the catalysts (T0, TW0, TW5, TW10 and TW15). The equation is as follows [17]:

$$(\alpha h\nu)^{\frac{1}{n}} = A\,(h\nu - E_g) \quad (2)$$

where α is the absorbance coefficient; $h\nu$ is the photon energy; A is a Tauc material property coefficient and an energy-independent constant; and E_g is the energy gap. The optical band gaps of the semiconductors T0, TW0, and TW were determined by extrapolating the straight section of the plot of (αh) and the straight section of the plot of $(\alpha h\nu)^{1/2}$ versus photon energy (Table 1).

Catalysts	λ (nm)	E_g reported (eV)	E_g obtained (eV)
T0	405	3.15 [14]	3.27
TW5	414	3.25 [18]	3.11
TW10	418	2.9 [19]	3.11
TW15	411	3.18 [18]	3.16

Table 1. Band gap energy values for the catalysts.

Figure 6 shows the optical band energy of the catalysts. The T0 sample has a band gap of 3.27 eV, consistent with the findings reported in the literature [14]. In the case of the TW5 and TW10 catalysts, they have a similar optical band gap (3.11 eV), while the case of the TW15 catalyst has an optical band gap of 3.16 eV.

The literature [20 - 22]photoluminescence, UV-Vis, and DRS spectroscopies; and by tensile tension tests. Results showed the successful formation and impregnation of NPs on the cotton fabric, with negligible leaching of NPs after several washing cycles. The photocatalytic activity of supported NPs was assessed by the degradation of methyl blue dye (MB indicates that the prohibited band gap of a crystalline semiconductor is related to the crystallite and particle size. When these are smaller, the energy band gap increases. This is consistent with the results of previous XRD studies, which reported an energy band gap of ~3.1 eV for TW catalysts. H. Lin and colleagues [21]3.8–5.7 nm propose that this is due to the spatial confinement of charge carriers, which results in the e^- and h^+ in the semiconductor being confined in a potential well.

On the other hand, the reduction in the energy band gap suggests a potential interaction between tungsten oxide and titania. The objective is to minimize the recombination of e^- and h^+ in the TW photocatalysts (TiO_2-WO_3). This could be

achieved by allowing electrons in the conduction band (CB) of titania to diffuse into the CB of tungsten. This process could be observed in the TW catalysts, potentially leading to enhanced photocatalytic activity.

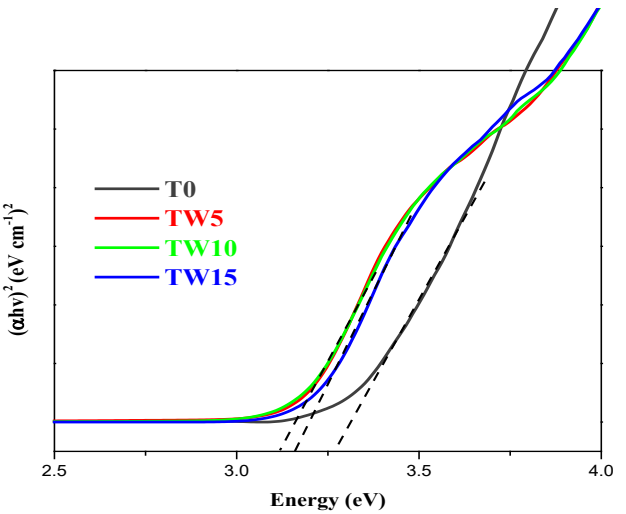

Figure 6. Optical band energies of the TiO_2 (T0) and TiO_2-WO_3 catalysts (TW).

3.3. *Photocatalytic evaluation of catalysts*

The catalysts were evaluated in two photocatalytic processes: the photocatalytic production of hydrogen and the decomposition of methyl orange (MO) (Figure 7a). The reaction kinetics of the photodegradation of organic pollutants is described by the Langmuir-Hinshelwood model [23]electrochemistry, analytical chemistry, radiochemistry, material chemistry, surface science, electronics, and hopefully catalysis. Since heterogeneous photocatalysis belongs to catalysis, all the bases of this discipline must be respected: (i. The rate constant (*kapp*) is the kinetics parameter that allows the determination of the photocatalytic activity independently of the adsorption process and the concentration of the remaining solute in the solution. In the case of these photocatalysts applied in the decomposition of MO, first-order kinetics was approximated and is described by equation (3):

$$\ln ln \frac{C}{C_0} = - kt \qquad (3)$$

The results of the analysis of the apparent reaction constant (*kapp*) of the catalysts T0 and TW, irradiated in UV and UV-Vis, are shown in Table 2. The R^2 values indicate that these catalysts present a first-order model, which means

that the degradation rate depends mainly on the amount of dye molecules in the solution [19]. The photocatalytic activity is compared by the value of the apparent rate constant, which is shown in Figure 7a. As expected, the highest *kapp* value was obtained for the TW15 catalyst, with a value of 0.0266 min^{-1}, showing a higher photocatalytic performance than the other photocatalysts in this reaction.

The TW15 photocatalyst offers a relatively large E_g, small crystal size, and large surface area (Table 1), which sets it apart from other photocatalysts; on the other hand, it also exhibits a higher photocatalytic activity, which corroborates the homogeneous dispersion of the titanium oxide and tungsten oxide particles. These results demonstrate the formation of a TiO_2-WO_3 heterojunction, which benefits the photocatalytic activity of titania for the degradation of dyes. According to the photoexcitation mechanism [24]I systematically discuss the properties of hetero junction photocatalysts in all cases. The formation of space charge regions, built-in electric field and potential barriers at the interface regions of thermally equilibrated heterojunctions are analyzed in details. When the heterojunctions are used for photocatalysis, the transfer behavior and mechanism of photo-excited non-equi librium carriers between the constituent semiconductors are discussed. It is demonstrated that the heterojunction properties, carrier transfer behavior and photocatalytic mechanism depend highly on the semiconductivity (Ntype or P-type, the e^- from the CB of titania is diffusing to the CB of WO_3. The WO_3 acts as an acceptor of e^- from the CB of titania, while the photogenerated h^+ from WO_3 migrates to the VB of titania, separating the electron-hole pair.

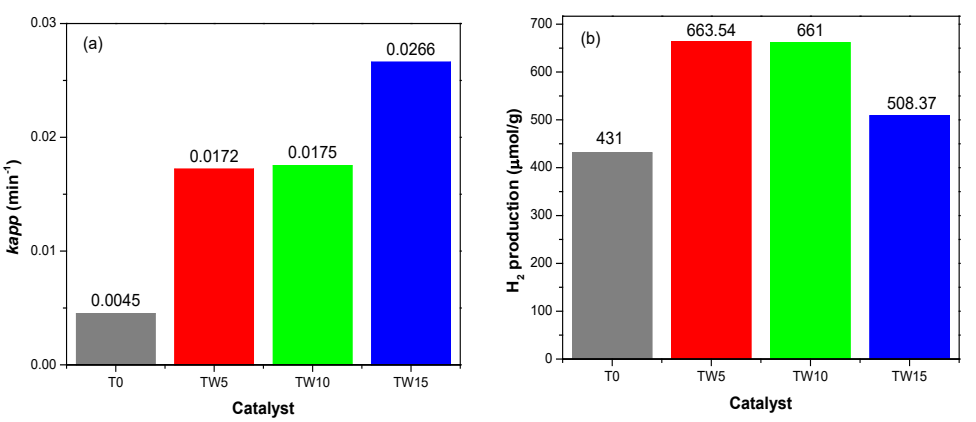

Figure 7. a) Apparent rate constant of catalysts in MO degradation; b) Catalytic evaluation of H_2 evolution of T0 and TW.

Also, Figure 7b compares the T0 sample with the TW catalysts for H_2 evolution using methanol (CH_3OH) as a sacrificial agent under UV-Vis irradiation for 4 h of reaction. The use of methanol as a sacrificial agent in the hydrogen production reaction serves two main purposes: 1) It has been reported that H_2 production increases considerably using methanol as a sacrificial agent, and 2) by performing this methanol degradation, the decomposition occurs, and the methanol is mineralized into less toxic substances [25].

This investigation demonstrates a higher H_2 generation in tungsten-containing catalysts. This research used a mixture of water and methanol with a 1:1 ratio; the methanol acted as a hydrogen ion scavenger. Figure 7b shows that the lower activity of T0 for H_2 generation was due to lower absorption of visible light. It is also important to note that it has a higher recombination rate of e^-/h^+. Adding WO_3 as a co-catalyst led to an improvement in the activity of TiO_2. In the presence of 5 %wt. of WO_3, an H_2 production of 663.54 μmol/g was achieved within 4 h, followed by the TW10 catalyst with an H_2 production of 661 μmol/g. This improvement can be attributed to the catalyst's ability to produce hydrogen rapidly. This improvement can be attributed to the fast charge separation observed in the case of the TW5 catalyst. In this case, using a sacrificial agent reduces the amount of WO_3 required in the sample, resulting in enhanced photocatalytic hydrogen production activity.

Particle size is a crucial factor in hydrogen production. It has been observed that smaller nanoparticles can exhibit higher photocatalytic activity compared with larger particles. In some cases, the small size of nanoparticles can give rise to a quantum effect. This results in the widening of the band gap [26], which, in turn, is related to a higher number of active sites on the smaller nanoparticles, allowing a higher exposure of these active sites to the reactant. Additionally, there is a higher interaction with the adsorbed molecules [27].

Finally, it can be observed that as the %wt. of WO_3 increases, the production of H_2 decreases; this can be observed in the TW15 catalyst, which catalyst has higher photocatalytic activity. However, the same does not happen to produce H_2; this could be attributed to the fact that there is a higher WO_3 charge, and it could possibly be acting as a shield effect and creating charge recombination centers, which subsequently decreases the evolution of H_2. In other words, the decrease of the H_2 could be due to three factors: 1) electronic band structure [28], 2) charge recycling [29], or 3) adsorption of species on the surface of the material [29]. The 15% wt incorporation of WO_3 into the heterojunction may alter these

band structures, affecting the availability of electronic states needed to facilitate the H_2 production reaction. It could also be because the tungsten could obstruct the transfer of e^- or h^+ across the interface between the two semiconductors.

According to the results, we can propose a reaction mechanism related to the activation of TiO_2-WO_3 heterojunction under UV-Vis light irradiation for MO degradation and hydrogen evolution. To know the VB and CB of the heterojunction between titania and tungsten, we used the Mott-Shottky diagram (Figure 8) and calculated from empirical formulae [24]I systematically discuss the properties of hetero junction photocatalysts in all cases. The formation of space charge regions, built-in electric field and potential barriers at the interface regions of thermally equilibrated heterojunctions are analyzed in details. When the heterojunctions are used for photocatalysis, the transfer behavior and mechanism of photo-excited non-equi librium carriers between the constituent semiconductors are discussed. It is demonstrated that the heterojunction properties, carrier transfer behavior and photocatalytic mechanism depend highly on the semiconductivity (Ntype or P-type using the equations:

$$E_{VB}=\chi-E_e+0.5\,E_g \qquad (4)$$

$$E_{CB}=E_{VB}-E_g \qquad (5)$$

where χ is the electronegativity of the material, E_{VB} is the VB potential, E_{CB} is the CB potential, E_g is the bandgap energy of the semiconductor, E_e is the energy of the free electrons (4.5 V). From this it can be seen that the E_{VB} of TiO_2 is 2.68 eV, and its E_{CB} is -0.24 eV; while, for the case of WO_3, its E_{VB} is 3.64 eV and its E_{CB} is 0.54 eV.

Catalyst	*kapp* (min^{-1})	R^2	H_2 production (μmol/g)
T0	0.0045	0.9764	431
TW5	0.0172	0.9712	663.54
TW10	0.0175	0.9669	661
TW15	0.0266	0.9301	508.37

Table 2. Apparent rate constant values for OM degradation and H_2 evolution.

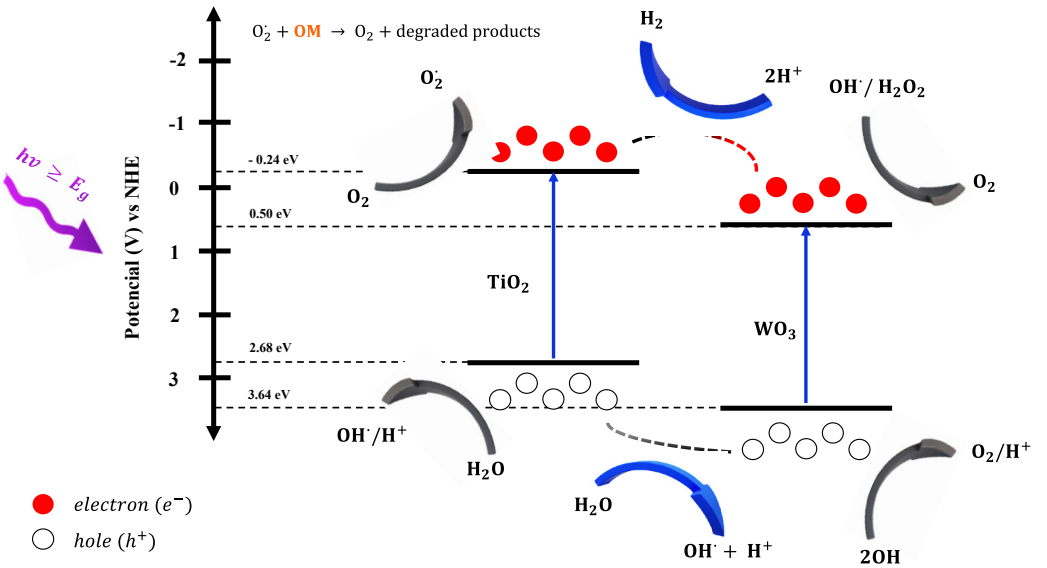

Figure 8. Mechanism of TiO_2-WO_3 heterojunction under UV-Vis.

4. Conclusions

Catalysts with a TiO_2-WO_3 heterojunction were synthesized by a hydrothermal method, modifying the tungsten oxide content (WO_3 % wt). The structural, morphological, and optical properties and chemical composition of the samples were investigated using different methods such as XRD, Raman, SEM, and UV-Vis.

XRD analysis showed that the anatase phase of TiO_2 predominates in samples T0, TW5, TW10, and TW15. The presence of WO_3 was not observed in XRD, so these species are smaller than 3 nm or highly dispersed on the titania surface. Raman showed the characteristic vibrational modes of TiO_2 at 142, 196, 396, 517, and 639 cm^{-1}; however, a shift towards higher frequencies was observed in the main band 142 cm^{-1} for the case of the TW catalysts, suggesting that this shift indicates that there could be a heterojunction between TiO_2 and WO_3, there could be some changes in the titania structure due to the incorporation and increase of WO_3. Also, for the TW10 and TW15 catalysts, we observed the signal at 966 cm^{-1}, which corresponded to the WO_x clusters and the W=O vibrational mode.

Using SEM, it was observed that the morphologies of the catalysts are irregular agglomerates, which could be attributed to the acid hydrolysis in the sol-gel phase of the synthesis and to the pH that we would obtain, since, according to the

literature, pHs lower than 5 are characteristic of agglomerated morphologies in these materials. The HRTEM analyses indicated that the particle size decreases as the tungsten oxide increases; also, by HAADF, it was observed that WO_3 is present in the form of small clusters of WOx deposited on the TiO_2 crystals, showing the formation of the heterojunction.

Using UV-Vis, it was observed that T0 absorbs in the UV region and, in the case of the TW catalysts, begins to absorb towards the visible region. In turn, the optical band energy of the catalysts was determined. The band gap energy value for the commercial sample (T0) was obtained according to the literature at about 3.27 eV. In the case of the TW5 and TW10 catalysts, the values slightly diminished at 3.11 eV and TW15 with 3.16 eV, showing that the particle size is important; the smaller the particle size, the higher the optical band energy. For the photocatalytic H_2 evolution, the TW5 catalyst presented a higher H_2 evolution because the band gap energy is narrow and the heterojunction between TiO_2 and WO_3 separates the e^-/h^+ pairs, however, for the TW10 and TW15 catalysts, although they presented a higher photocatalytic activity, they did not present a higher H_2 evolution, this could be because there is a higher WO_3 charge and possibly it would be working as a shielding effect and create charge recombination centers which subsequently reduce the H_2 evolution.

Acknowledgments

This work was funded by SIP-20240532 and SIP-20230974, a project funded by the Instituto Politécnico Nacional - Mexico. The authors thank the CNMN-IPN for the characterization of the materials. Xochiquetzalli González Bautista thanks CONAHCyT - Mexico for the PhD scholarship.

References

1. Lewis, N. S., & Nocera, D. G. (2006). Powering the planet: Chemical challenges in solar energy utilization. *Proceedings of the National Academy of Sciences, 103*(43), 15729–15735. https://doi.org/10.1073/pnas.0603395103

2. Holladay, J. D., Hu, J., King, D. L., & Wang, Y. (2009). An overview of hydrogen production technologies. *Catalysis Today, 139*(4), 244–260. https://doi.org/10.1016/j.cattod.2008.08.039

3. Hisatomi, T., & Domen, K. (2019). Reaction systems for solar hydrogen production via water splitting with particulate semiconductor photocatalysts. *Nature Catalysis, 2*(5), 387–399. https://doi.org/10.1038/s41929-019-0242-6

4. Kudo, A., & Miseki, Y. (2009). Heterogeneous photocatalyst materials for water splitting. *Chemical Society Reviews, 38*(1), 253–278. https://doi.org/10.1039/B800489G

5. Pinaud, B. A., Benck, J. D., Seitz, L. C., Forman, A. J., Chen, Z., Deutsch, T. G., et al. (2013). Technical and economic feasibility of centralized facilities for solar hydrogen production via photocatalysis and photoelectrochemistry. *Energy & Environmental Science, 6*(7), 1983–2002. https://doi.org/10.1039/c3ee40831k

6. Toledo Camacho, S. Y., Rey, A., Hernández-Alonso, M. D., Llorca, J., Medina, F., & Contreras, S. (2018). Pd/TiO2-WO3 photocatalysts for hydrogen generation from water-methanol mixtures. *Applied Surface Science, 455*, 570–580. https://doi.org/10.1016/j.apsusc.2018.05.122

7. Kim, Y. H., Park, H., Kim, S., Jeong, H., Lee, C., Shin, S., et al. (2020). Directional change of interfacial electric field by carbon insertion in heterojunction system TiO2/WO3. *ACS Applied Materials & Interfaces, 12*(13), 15239–15245. https://doi.org/10.1021/acsami.0c00669

8. Wan, J., Chen, X., Zeng, C., Zhong, X., Xu, Z., Jiang, D., et al. (2018). Defect effects on TiO2 nanosheets: Stabilizing single atomic site Au and promoting catalytic properties. *Advanced Materials, 30*(11), 1705369. https://doi.org/10.1002/adma.201705369

9. Zhu, J., Liu, Z., Yang, F., Long, D., Jian, Y., & Pu, S. (2022). The preparation of {001} TiO2/TiOF2 via a one-step hydrothermal method and its degradation mechanism of ammonia nitrogen. *Materials, 15*(18), 6465. https://doi.org/10.3390/ma15186465

10. Liu, X., Du, G., & Li, M. (2019). True photoreactivity origin of Ti3+-doped anatase TiO2 crystals with respectively dominated exposed {001}, {101}, and {100} facets. *ACS Omega, 4*(12), 14902–14912. https://doi.org/10.1021/acsomega.9b01648

11. Basumatary, B., Basumatary, R., Ramchiary, A., & Konwar, D. (2022). Evaluation of Ag@TiO2/WO3 heterojunction photocatalyst for enhanced photocatalytic activity towards methylene blue degradation. *Chemosphere, 286*, 131848. https://doi.org/10.1016/j.chemosphere.2021.131848

12. Yuan, Y., Tian, J., Zhao, H., Zhang, Q., Zhang, X., Li, Q., & Zhao, L. (2021). A review of metal oxide-based Z-scheme heterojunction photocatalysts: Actualities and developments. *Materials Today Energy, 21*, 100829. https://doi.org/10.1016/j.mtener.2021.100829

13. Tian, F., Zhang, Y., Zhang, J., & Pan, C. (2012). Raman spectroscopy: A new approach to measure the percentage of anatase TiO2 exposed (001) facets. *The Journal of Physical Chemistry C, 116*(13), 7515–7519. https://doi.org/10.1021/jp301256h

14. Doševic-Mitrovic, Z., Jankovic, S., Živković, J., Cvjetićanin, N., & Grguric-Sipka, S. (2016). WO3/TiO2 composite coatings: Structural, optical and photocatalytic properties. *Materials Research Bulletin, 83*, 217–224. https://doi.org/10.1016/j.materresbull.2016.06.011

15. Gutiérrez-Alejandre, A., Ramírez, J., & Busca, G. (1998). A vibrational and spectroscopic study of WO3/TiO2-Al2O3 catalyst precursors. *Langmuir, 14*(3), 630–639. https://doi.org/10.1021/la970993n

16. Leghari, S. A. K., Sajjad, S., Chen, F., & Zhang, J. (2011). WO3/TiO2 composite with morphology change via hydrothermal template-free route as an efficient visible light photocatalyst. *Chemical Engineering Journal, 166*(3), 906–915. https://doi.org/10.1016/j.cej.2010.11.065

17. Dolgonos, A., Mason, T. O., & Poeppelmeier, K. R. (2016). Direct optical band gap measurement in polycrystalline semiconductors: A critical look at the Tauc method. *Journal of Solid State Chemistry, 240*, 43–48. https://doi.org/10.1016/j.jssc.2016.05.010

18. Habtamu, A., & Ujihara, M. (2023). The mechanism of water pollutant photodegradation by mixed and core–shell WO3/TiO2 nanocomposites. *RSC Advances, 13*(19), 12926–12940. https://doi.org/10.1039/D3RA01582C

19. Pinedo-Escobar, J. A., Fan, J., Moctezuma, E., Gomez-Solís, C., Carrillo Martinez, C. J., & Gracia-Espino, E. (2021). Nanoparticulate double-heterojunction photocatalysts comprising TiO2(Anatase)/WO3/TiO2(Rutile) with enhanced photocatalytic activity toward the degradation of methyl orange under near-ultraviolet and visible light. *ACS Omega, 6*(18), 11840–11848. https://doi.org/10.1021/acsomega.0c06054

20. Chacon-Argaez, U., Pacheco-Sánchez, J. H., & May-Pat, A. (2023). Photocatalytic activity and biocide properties of Ag–TiO2 composites on cotton fabrics. *Materials, 16*(13), 4513.
https://doi.org/10.3390/ma16134513

21. Lin, H., Huang, C., Li, W., Ni, C., Shah, S., & Tseng, Y. (2006). Size dependency of nanocrystalline TiO2 on its optical property and photocatalytic reactivity exemplified by 2-chlorophenol. *Applied Catalysis B: Environmental, 68*(1–2), 1–11.
https://doi.org/10.1016/j.apcatb.2006.07.018

22. Kumar, S., Verma, N. K., & Singla, M. L. (n.d.). Size dependent reflective properties of TiO2 nanoparticles and reflectors made thereof.

23. Herrmann, J.-M. (2010). Photocatalysis fundamentals revisited to avoid several misconceptions. *Applied Catalysis B: Environmental, 99*(3–4), 461–468.
https://doi.org/10.1016/j.apcatb.2010.05.012

24. Yang, H. (2021). A short review on heterojunction photocatalysts: Carrier transfer behavior and photocatalytic mechanisms. *Materials Research Bulletin, 142*, 111406.
https://doi.org/10.1016/j.materresbull.2021.111406

25. Pulido Melián, E., et al. (2013). Efficient and affordable hydrogen production by water photo-splitting using TiO2-based photocatalysts. *International Journal of Hydrogen Energy, 38*(5), 2144–2155.
https://doi.org/10.1016/j.ijhydene.2012.12.005

26. Kudo, A., & Miseki, Y. (2009). Heterogeneous photocatalyst materials for water splitting. *Chemical Society Reviews, 38*(1), 253–278.
https://doi.org/10.1039/B800489G

27. Suresh, R., Gnanasekaran, L., Rajendran, S., & Soto-Moscoso, M. (2023). Doped nanomaterials: Application in hydrogen production via photocatalytic water splitting. *Fuel, 348*, 128528.
https://doi.org/10.1016/j.fuel.2023.128528

28. Hao, Y., et al. (2021). Energy band engineering and interface transfer strategies to optimize photocatalytic hydrogen evolution performance. *Applied Surface Science, 546*, 149137.
https://doi.org/10.1016/j.apsusc.2021.149137

29. Xu, J., et al. (2024). Recent advances in heterogeneous catalysis of solar-driven carbon dioxide conversion. *Journal of Environmental Sciences, 140*, 165–182.
https://doi.org/10.1016/j.jes.2023.06.028